Chemical Engineering Science 245 (2021) 116937

Contents lists available at ScienceDirect

Chemical Engineering Science

journal homepage: www.elsevier.com/locate/ces

Modelling bed dimension for fluidized bed chemical vapour deposition

Young Mi Chung

School of Energy, Materials & Chemical Engineering, Korea University of Technology and Education, Chungjeol-ro 1600, Byeongcheon-myeon, Dongnam-gu, Cheonan-si, Chungcheongnam-do, Republic of Korea

HIGHLIGHTS

- An analytical model for bed dimension of a FCVD process is proposed.
- The proposed model defines relationships among process variables.
- The proposed model can help manipulate process variables within their limits.
- The proposed model can serve as a guideline for scale-up of a FCVD column.

GRAPHICAL ABSTRACT

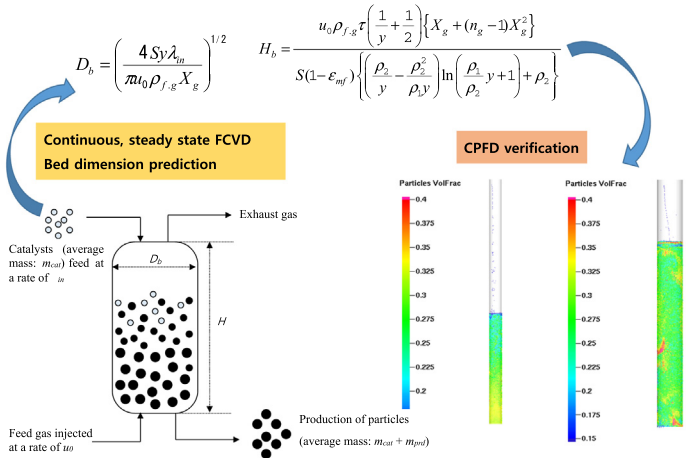

ARTICLE INFO

Article history:
Received 8 December 2019
Received in revised form 4 July 2021
Accepted 6 July 2021
Available online 9 July 2021

Keywords:
Fluidization
FBCVD
CPFD
Scale-up
Dimension

ABSTRACT

The present paper introduces a simple analytical model to predict the bed dimension of a continuous FBCVD (fluidized bed chemical vapour deposition) process. The expressions for column diameter and bed height were determined based on the target production rate, yield, conversion of the feed gas and gas volume change in the system. The model proposed in this article suggests that the diameter of an FBCVD column has to be reduced to enhance the conversion at a given production rate. To avoid linear expansion of the column diameter upon scale-up, the conversion or the superficial velocity of the feed gas has to increase, which results in an increase in the bed height. On the basis of the proposed model, a reasonable preliminary column dimension can be outlined when only a limited number of process parameters are available. CPFD (computational particle fluid dynamics) simulation results are presented to verify the model.

1. Introduction

Fluidization is an important process that enables large-scale production of value-added solid products with effective heat and mass transfer. Bed fluidization processing has found applications in chemical vapour deposition (CVD) processes for various fine solid particles, such as carbon nanotubes, SiO_2, and SnO_2 (Caussat et al., 1995; Filtvedt et al., 2010; Hua and Li, 1999; Morooka et al., 1990; See and Harris, 2007). CVD process is widely used specially in solid thin film coatings, high purity bulk powdery materials and fabricating composite materials, etc (Creighton and Ho, 2001). During the CVD process, a precursor gas or gas mixture is

E-mail address: quebecoise@koreatech.ac.kr

https://doi.org/10.1016/j.ces.2021.116937
0009-2509/

Nomenclature

A	reactor cross-sectional area, (m^2)
D_b	bed diameter, (m)
d_{cat}	average diameter of catalyst, (m)
d_p	particle diameter, (m)
g	gravitational acceleration, (m^2/s)
H	fluidization height, (m)
m_{cat}	mass of a catalyst, (kg)
m_{prd}	mass of the deposited solid product on a catalyst, (kg)
$\bar{m}_{bed}$	time-averaged bulk weight of particles in the bed, (kg)
$\overline{m}_{bad}$	time-averaged weight of a particle in the bed, (kg)
$\overline{m}_{cat}$	time-averaged weight of a catalyst particle, (kg)
$\overline{m}_{out}$	time-averaged weight of a catalyst + product particle in the system, (kg)
$\bar{n}_{bed}$	time-averaged number of particles in the reactor, (–)
n_g	stoichiometric coefficient of by-product gas, (–)
ΔP_b	pressure drop of a fluidized bed with gas expansion due to the reaction, (Pa)
ΔP_b^0	pressure drop of a fluidized bed without gas expansion, (Pa)
S	stoichiometric ratio, (kg/kg)
u_0	superficial linear velocity of feed gas into the reactor, (m/s)
V_{cat}	volume of a catalyst, (m^3)
V_{prd}	volume of the deposited solid product on a catalyst, (m^3)
X_g	actual conversion of the feed gas, (kg/kg)
y	target yield after residence time, (kg/kg)
$\dot{y}$	instantaneous yield at time t, (kg/kg)

Greek Letters

δ	gas expansion factor, (–)
ε	apparent bed voidage, (–)
ε_{mf}	bed voidage at minimum fluidizing conditions, (–)
μ	viscosity of the gas mixture, (Pa.s)
λ_{in}	weight-averaged input velocity of particles, average feed rate of catalyst, (kg/s)
λ_{out}	weight-averaged output velocity of particles (production rate), average target production, (kg/s)
ρ_{cat}	density of a catalyst, (kg/m^3)
ρ_{prd}	density of the deposited solid product on a catalyst, (kg/m^3)
ρ_g	density of gas mixture in the system at reaction temperature, (kg/m^3)
$\rho_{f\cdot g}$	density of the feed gas at reaction temperature, (kg/m^3)
ρ_s	density of solid (catalyst + product) particles, (kg/m^3)
$\dot{\rho}_s$	density of a solid particle at time t, (kg/m^3)
$\bar{\rho}_s$	average density of particles in the system, (kg/m^3)
τ	average residence time of particles in the system, (s)
υ_{in}	number-averaged input velocity of particles, (s^{-1})
υ_v	volumetric velocity of feed gas into the reactor, (m^3/s)
υ_w	weight-based input rate of feed gas into the reactor, (kg/s)
ϕ_s	sphericity of particles, (–)

injected into a column, where heated particles such as catalysts are to be deposited after chemical reactions with the injected gas on their surface as shown in Fig. 1(a). The exhaust gas, which is by-product from the chemical reactions, would eventually exit the system along with the unreacted residual precursor gas. The resultant product should be particles with a thin film on the surface of the heated particles.

As there are large variety of materials deposited and wide range of applications, there are many variants of CVD. The process can operate in either hot-wall columns or cold-wall column. The process condition can adopt above-atmospheric or below-atmospheric pressure, with or without carrier gases, and at temperatures typically ranging from 200 to 1600 °C (Creighton and Ho, 2001). One of the earliest application of a large-scale CVD was a carbonyl process for refining nickel (Mond et al., 1890). Many early applications involve refining or purification of metals and some number of non-metals products through carbonyl or halide processes (Powell et al., 1966). Other early applications include deposition of coatings for wear and corrosion resistance, and the fabrication of structural shapes and components (Powell et al., 1966). Although, many high volume applications, including refining and the production of powders and pigments, are still important economically, most recent applications focus on film deposition. For example, synthesis of metastable diamond film under low-pressure has been an important application of CVD due to high thermal conductivity, chemical inertness, or electronic properties of diamond (Lee et al., 1999). Also, a lot of CVD research has been going on in the area of semiconductor (Mills et al., 2002; Neudeck, 1995; Berenbaum et al., 2021; Batey et al., 1989). For example, CVD processes have been applied to deposit thin films of the active semiconductor material such as doped Si (Neudeck, 1995) or conductive (Berenbaum et al., 2021) or insulating materials (Batey et al., 1989).

The CVD techniques do not always involve FBR (Fluidized Bed Reactor) system. SIEMENS adopted a bell-jar system for their polysilicon production (Guenther et al., 2001). A cold wall rotating disk CVD reactor was adopted for silicon or compound semiconductor production (Breiland et al., 1999; Breiland and Evans, 1991). Gas fluidization of solid particles, however, offers several advantages: first, fluidized beds are generally near-perfectly isothermal; second, particles are thoroughly mixed, which results in a near-perfect uniformity of surface treatment (Caussat et al., 1995). Also, production through FBCVD is advantageous due to the low production cost, low energy consumption and high productivity (Jianlong et al., 2011). In fact, there have been a number of cases adopting Fluidization system for CVD reaction. Wood et al. (1991) attempted aluminium or titanium coatings on mica through FBCVD. Cadoret et al. (2009) deposited silicon onto titanium oxide powders. Hua and Li produced the nanocrystalline SnO_2 films on Al_2O_3 particles by FBCVD (Hua and Li, 1999). Morooka et al. (1989) have deposited TiN either on agglomerates of Si_3N_4 nanoparticles, or on agglomerates of Al_2O_3 nanoparticles. King et al. (2007) reports that ALD (atomic layer deposition) can be performed in a fluidized bed under low pressure, to coat micro- and nanometer particles by alumina (Al_2O_3). Sanjurjo et al. (1992) listed a number of coating materials such as Si and Ti or Cu substrates in a FBR. Zhang et al. (2010) produced carbon nanotube (CNT) using Fe/Mo/vermiculite catalysts in a FBCVD system. Also, a number of researchers has also studied pyrolysis of silane for silicon film growth using FBCVD system (Filtvedt et al., 2010, 2013; Hua and Li, 1999; Tejero-Ezpeleta et al., 2004; Furusawa et al., 1988).

Even with a number of advantages and applications of FBCVD processes, to the author's best knowledge, there has been no clear guideline on the column dimensions for FBCVD systems so far. Although several efforts have been made in modelling of FBCVD

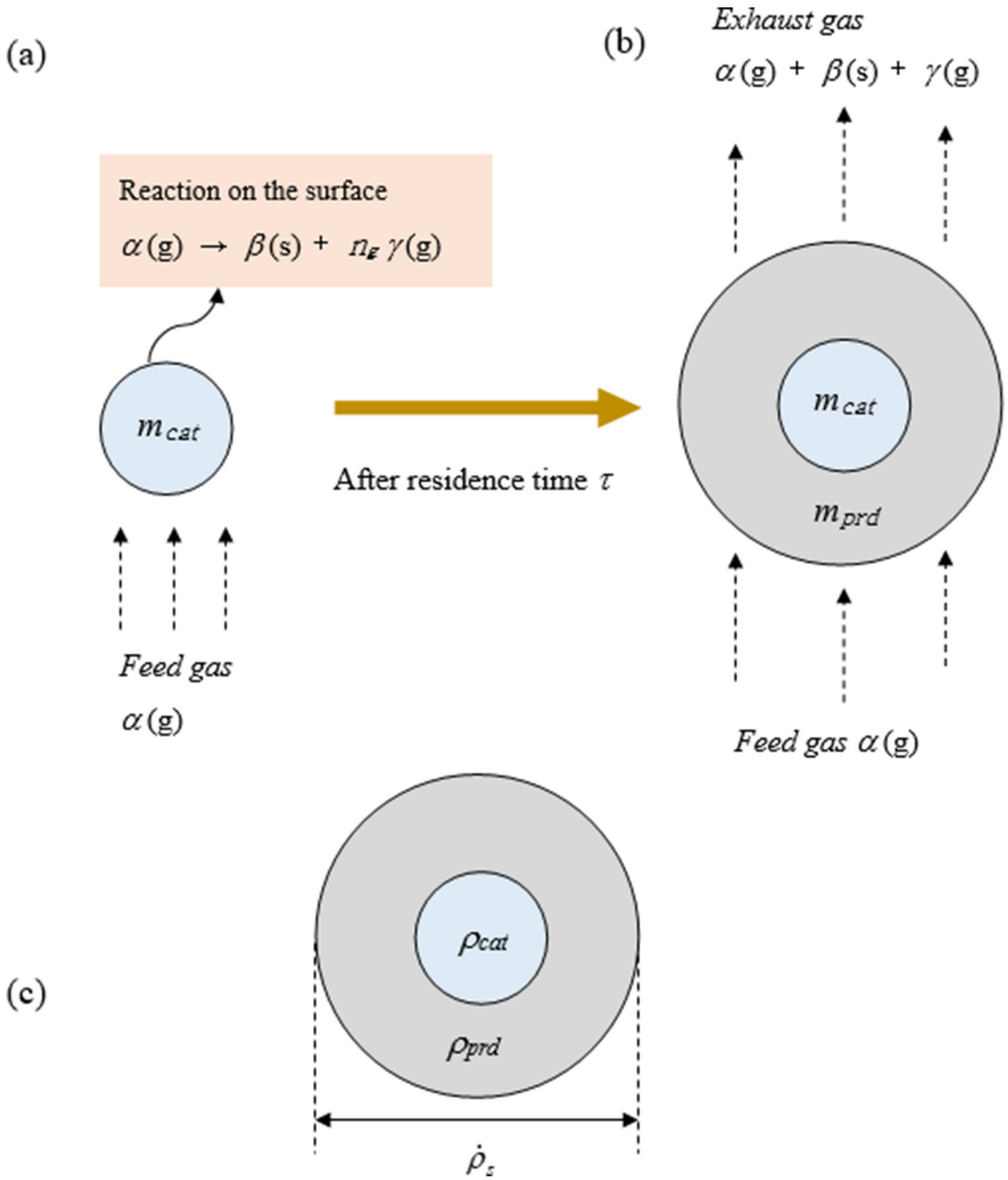

Fig. 1. Schematic presentation of (a) mass of a catalyst and the reaction on the surface (b) mass of a catalyst + product, feed gas and exhaust gas (c) density of a catalyst + product at time *t* during CVD growth.

(Calderbank and Toor, 1971; Partridge and Rowe, 1966; Horio and Wen, 1977); these models are mostly focusing on the prediction of microscopic phenomena such as bubble size distribution. However, for the best productivity, the bed dimension has to be carefully modelled and optimized before studying inner complex events. Mostly, process engineering and scale-up of these processes are carried out without much effort into preliminary calculations or optimization. Therefore, performing process optimization without fully understanding the underlying principles often leads to a trial-and-error approach to the problem and hence results in a waste of time and cost.

In the present study, a simple analytical model is presented to help design an FBCVD column at the initial basic engineering step. The model derived herein is based on the theoretical expression for minimum fluidising systems. At higher feed gas rate, for example, for bubbling or slugging conditions, one may have to give extra margin to the bed dimension by increasing the column height. Also, depending on the changes in gas volume of the bed due to the CVD reaction, some adjustments to the bed dimension would be necessary.

The derivation of bed dimension was done analytically and verified through CPFD (computational particle fluid dynamics, commercial name Barracuda®, Albuquerque, USA) simulations. For most simulation studies for fluidized bed system, both Eulerian-Eulerian two fluid model (TFM) and Eulerian-Lagrangian discrete element model (DEM) have been adopted (Wu et al., 2018). TFM has its own limitation as it treats gas and solid as interpenetrating continua and thus discrete solid particles cannot be considered. Consequently, TFM cannot account for particle size distribution or shear stress of the particles. DEM treats the fluid phase as a continuum by solving time-averaged Navier-Stokes equations, while the particle phase is described by the Newton equation (Wu

et al., 2018). Unlike the TFM, each particle can be tracked individually and also the interaction between particle/particle and particle/fluid can be calculated. However, using DEM method to describe a fluidized bed system with numerous number of particles is virtually impossible as DEM can handle only limited number of particles on the order of $2^{*}10^{5}$ (Shi et al., 2014).

CPFD is an efficient way of simulating a large-scale particle system (Snider et al., 2011), based on Eulerian-Lagrangian scheme with the MP-PIC (multi-phase-particle in cell) method. The CPFD method is a hybrid numerical method, in which the fluid phase is calculated with an Eulerian computational grid and the solids are predicted using Lagrangian computational particles or parcel-of particles in which particles are grouped with the same properties such as size, density, velocity, residence time, etc (Snider, 2007). Thanks to its parcel of particles method, CPFD can simulate large-scale system with billions of particles in relatively short time compared to other tools. Therefore, CPFD, in terms of computational cost and time, is the best tool to describe a fluidized bed system, which always involves numerous particles.

All column dimensions tested herein with CPFD can also be realized experimentally. However, it is very expensive to build each and every column of different dimensions. Moreover, for some catalytic reactions conducted at high temperature in an FBCVD system, it is very difficult to visualize the particle dynamics occurring inside the reactors. In this case, simulation is a superior tool to visualize and verify a process model. There are numerous reports that have verified the feasibility of the CPFD simulation method as a substitute for a real process (Abbasi et al., 2011; Cheng et al., 2012; Wang et al., 2014; Parker, 2011), which includes an example of simulation of FBCVD system for polysilicon deposition (Parker, 2011). Additionally, process simulations using CPFD can serve as an effective way of predicting system behaviour after scale-up.

2. Modelling

2.1. Definition of yield

For an FBCVD process, generally, a certain amount of fine catalyst particles is injected in through the upper part of a reactor, after which the reactant vapour is decomposed on the surface of the catalysts and converted to solid product. Therefore, the solid particles grow heavier with time, and after a certain residence time, the particles are to be harvested from the bottom of the reactor.

Here, imagine we have grown particles on catalysts of average mass m_{cat}, as depicted in Fig. 1. Additionally, imagine that, after a certain residence time, the gaseous reactant has been deposited as solid product of mass, m_{prd}, on the surface of the catalyst.

Let us define the yield (y) as below:

$$y = \frac{m_{prd}}{m_{cat}} \tag{1}$$

One needs to determine the value of y through a simple analysis of reaction kinetics, such as through a quartz boat experiment (Ni et al., 2006; Makris et al., 2005; Philippe et al., 2009). The final yield can be obtained by measuring the difference in mass between the catalysts and the final product particles after allowing the reaction to proceed for a designated residence time. Therefore, the ratio of the production rate (λ_{out}) to the catalyst input rate (λ_{in}) should be expressed as below:

$$\frac{\lambda_{out}}{\lambda_{in}} = \frac{m_{cat} + m_{prd}}{m_{cat}} = 1 + y \tag{2}$$

The yield term is both spatially averaged and time-averaged. Overall, harvested particles should exhibit the average yield over time. Particles may show different yields from one another and deviate from the average yield. However, the difference should be infinitesimal, given that catalyst particles are produced in such a fashion that the concentration and distribution of active sites on the catalysts are almost even.

2.2. Pressure drop

2.2.1. Model I: Fast reaction model

Fig. 2(a) is a simple illustration of an FBCVD system that depicts an ideal case of a very fast reaction with effective mixing. This simple, ideal model is based on the assumption that the reaction is so fast that a particle mass in the system is almost the same as that of an outflowing particle. Additionally, each particle resides inside the reactor for the residence time, and the number of inflowing particles is almost the same as that of outflowing particles, which indicates that the system is at steady state in terms of particle numbers. Therefore, the average number of particles in the bed can be expressed as follows:

$$\bar{n}_{bed} = \upsilon_{in}\tau \tag{3}$$

Here, $\bar{n}_{bed}$ and υ_{in} indicate the time-averaged number of particles in the reactor and the number-averaged input velocity of particles, respectively. τ is the average residence time of particles in the system. The time averaged number of particles in the bed should equal the time averaged bulk weight of the bed divided by the average weight of particles. Also, the number-averaged input velocity equals the weight-averaged velocity divided by the average weight of the particles. Therefore, Eq. (3) can be replaced with

$$\frac{\bar{m}_{bed}}{\bar{\dot{m}}_{bed}} = \frac{\lambda_{in}}{\bar{\dot{m}}_{cat}}\tau \tag{4}$$

where $\bar{m}_{bed}$ and $\bar{\dot{m}}_{bad}$ denote the time-averaged bulk weight of particles in the bed and time-averaged weight of a particle in the bed, respectively. $\bar{\dot{m}}_{cat}$ indicates the time-averaged weight of a catalyst particle. For a steady-state continuous system, the following relation is true.

$$\bar{\dot{m}}_{bed} = \bar{\dot{m}}_{out} \tag{5}$$

where $\bar{\dot{m}}_{out}$ indicates time-averaged weight of a catalyst + product particle in the system.

Eqs. (4) and (5) give

$$\bar{m}_{bed} = \lambda_{in}\tau\frac{\bar{\dot{m}}_{out}}{\bar{\dot{m}}_{cat}} \tag{6}$$

From Eq. (1),

$$\frac{\bar{\dot{m}}_{out}}{\bar{\dot{m}}_{cat}} = 1 + y \tag{7}$$

Solving Eqs. (6) and (7) simultaneously, cancelling the term $\bar{\dot{m}}_{cat}$ gives

$$\bar{m}_{bed} = \lambda_{in}\tau(1 + y) \tag{8}$$

We know that

$$\Delta P_b^0 = \frac{\bar{m}_{bed}g}{A} \tag{9}$$

where ΔP_b^0 indicates the pressure drop of a fluidized bed without gas expansion from CVD reaction. A is cross sectional area of the column and g is the gravitational acceleration.

Combining Eqs. (8) and (9) gives the expression for the pressure drop for system I as depicted in Fig. 2(a):

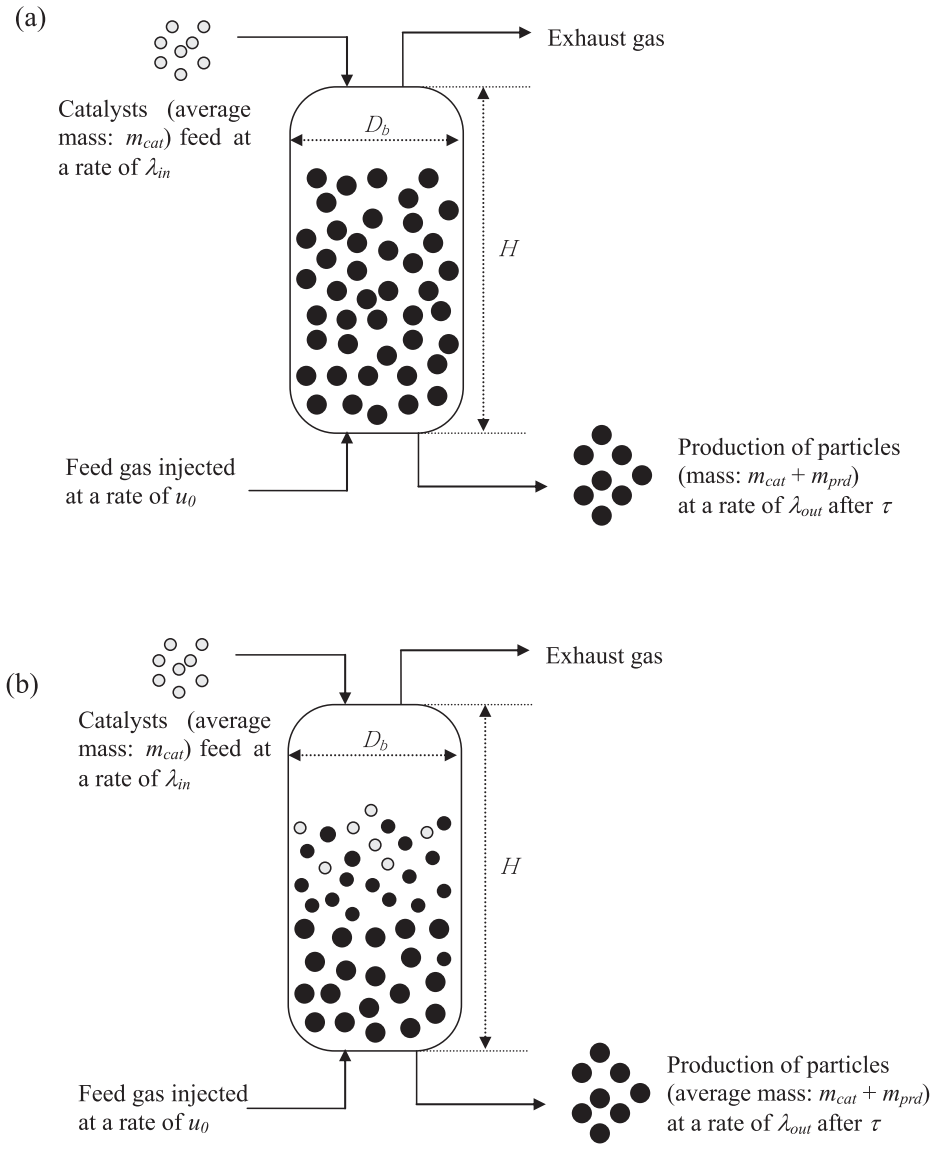

Fig. 2. Illustration of time averaged particles distribution of (a) fast reaction FCVD and (b) slow reaction FCVD.

$$\Delta P_b^{0(I)} = \frac{\lambda_{in}(1+y)\tau g}{A} = \frac{\lambda_{out}\tau g}{A} \tag{10}$$

As expected from the assumptions previously mentioned, this model should lead to an overestimation of bed pressure drop due to the premature particles in the system. To correct this issue, a more realistic model accounting for the particle size distribution of the bed is introduced below in Model II.

2.2.2. Model II: Slow reaction model

The system illustrated in Fig. 2(b) accounts for reactions similar to the real FCVD process. The reaction rate is relatively slow, and hence, there exist a considerable number of raw catalysts and small particles inside the reactor. The particle size shows an almost standard distribution, and after a certain residence time, the particles are harvested from the bottom. For the system depicted in Fig. 2(b), we start from Eq. (4). If the growth of one particle is considered, the average particle size is related to yield as below:

$$\overline{m}_{bed} = \frac{1}{\tau}\int_0^{\tau} \overline{m}_{cat}(1+\dot{y})dt \tag{11}$$

Here, $\dot{y}$ is the instantaneous yield at time t. The yield change is assumed to be linearly proportional to time as below:

$$\dot{y} = \left(\frac{y}{\tau}\right)t \tag{12}$$

Unlike in Model I, the yield is directly proportional to the productivity and thus can be assumed to be proportional to time for a very slow reaction such as carbon nanotube growth (Philippe et al., 2009). For a very slow reaction, it is hard to achieve high conversion within a reasonable period of residence time. In this case, the reaction rate is more affected by the quality of the catalysts than the hydrodynamic mixing efficiency of the surrounding fluid, especially at the minimum fluidization condition.

Obviously, Eq. (12) can be replaced by a more elaborate kinetics expression, such as a quadratic equation based on laboratory experimental data. One can adopt an appropriate expression of conversion versus reaction time. These elaborate forms of kinetic formulas may well explain the microscopic behaviour of chemical deposition at the reaction sites and work well at a laboratory scale. However, such formulas are not always expected to be successful in describing the overall bulk fluidization behaviour, mostly due to the accumulation of error from each reaction site. The kinetic model should be able to predict the target yield after a designated residence time in a large-scale column. Therefore, in this work, the reaction kinetics is limited to zero order kinetics, where the

production rate is assumed proportional to time, which is mostly the case with very slow reactions.

As $\overline{\dot{m}}_{cat}$ is independent of time, Eq. (11) becomes

$$\overline{\dot{m}}_{bed} = \overline{\dot{m}}_{cat}\left(1+\frac{y}{2}\right) \tag{13}$$

Solving (2), (4), (8) and (13) simultaneously gives the following expression for the pressure drop in terms of the target production rate, λ_{out}:

$$\Delta P_b^0 = \frac{\lambda_{in}\tau g\left(1+\frac{y}{2}\right)}{A} = \frac{\lambda_{out}\tau g\left(1+\frac{y}{2}\right)}{A(1+y)} = \frac{(1+0.5y)}{(1+y)}\Delta P_b^{0(I)} \tag{14}$$

A correction factor of $(1 + 0.5y)/(1 + y)$ was introduced into the above expression, in addition to the Model I pressure drop, $\Delta P_b^{0(I)}$. This correction factor is obviously less than one and thus corrects the overestimation of $\Delta P_b^{0(I)}$. However, when the yield is very low, the above correction factor converges to one, and thus the two models, Model I and Model II, become almost the same as there exist mostly raw catalysts in the two systems.

Eq. (14) does not consider the increase in drag force due to gas expansion during the CVD reaction. $\Delta P_b^{0(I)}$ indicates the bed pressure drop with no gas expansion and no change in particle size and density. The change in the total number of gas molecules during the reaction should affect the overall pressure drop of the bed, which will be discussed in Section 2.4 below. For now, we need an expression for the column cross-sectional area (A) in Eq. (14), which will be derived in the following section.

2.3. Column diameter

The expression for the column diameter can be derived from a simple mass balance as described below. The volumetric velocity of the feed gas is equal to the product of superficial velocity and the cross-sectional area of the reactor.

$$\upsilon_v = u_0 A \tag{15}$$

where υ_{in} volumetric velocity of feed gas into the reactor and u_0 is indicates the superficial linear velocity of feed gas into the reactor.

Eq. (15) can be rewritten in mass-based terms as follows:

$$\upsilon_w = u_0 A \rho_{f.g} \tag{16}$$

υ_w is the weight-based input rate of feed gas into the reactor and $\rho_{f.g}$ is the density of the feed gas at reaction temperature and Eq. (16) depicts the case without chemical reaction. When a reaction takes place, the mass balance for the fluidized bed should be expressed as follows:

[Rate of feed gas consumption (kg/s)] = [Rate of feed gas conversion into product (kg/s)]

Therefore, when a CVD reaction occurs with the conversion of the feed gas, X_g in the reactor, Eq. (16) becomes:

$$S(\lambda_{out} - \lambda_{in}) = u_0 A \rho_{f.g} X_g \tag{17}$$

The left-hand side of Eq. (17) refers to the steady state production rate (λ_{out} – λ_{in}) multiplied by the stoichiometric ratio (S). The stoichiometric ratio is the mass ratio of the reactant over the product when one mole of reactant gas has gone through the chemical reaction. Rearranging Eq. (17) gives:

$$A = \frac{S(\lambda_{out} - \lambda_{in})}{u_0 \rho_{f.g} X_g} \tag{18}$$

As $A = \frac{\pi}{4}D_b^2$,

$$D_b = \left(\frac{4S(\lambda_{out} - \lambda_{in})}{\pi u_0 \rho_{f.g} X_g}\right)^{1/2} = \left(\frac{4Sy\lambda_{in}}{\pi u_0 \rho_{f.g} X_g}\right)^{1/2} \tag{19}$$

All the parameters appearing on the right hand side of Eq. (19) are either physical properties or target values for the process design. For example, y is determined if you set the target productivity (λ_{out}), given the feed flow rate of catalyst (λ_{in}). Also, the superficial velocity, u_0 is not an arbitrary value but has to be determined from a reasonable range that allows minimum fluidization of the bed. S is already determined by the stoichiometric relation of the chemical reaction on the catalyst surface. $\rho_{f.g}$ is a physical property that one can either find from a data book or obtain from experiments. X_g is conversion of the feed gas that a process designer wants to achieve from the system. Note that X_g is not a dependent variable. It, rather, ultimately affects the dimension of a column. For instance, one needs to reduce the column diameter (D_b) if one wants to set higher conversion of the feed gas, X_g at a fixed production rate, as can also be inferred from Eq. (19). In this case, the column diameter should decrease and the bed height should increase to maintain the bed volume and the production rate. Furthermore, the column diameter decreases as the superficial velocity of the feed gas increases, which should result in a bed height increase. Another important perspective is that the column diameter should decrease when the reaction rate slows down. In other words, when dealing with poorly performing catalysts that always give a low yield (y), the column diameter should be downsized accordingly, as the column diameter is proportional to $y^{1/2}$ in Eq. (19).

2.4. Bed height

One needs to know the approximate bed height to determine the column height. Without knowing the fluidized bed height (H), one cannot design the column and the associated accessory facilities properly. The expression for the bed height was derived starting from a simple force balance exerted on a particle at minimum fluidization (Kunii and Levenspiel, 1991).

(Drag force by upward-moving gas) = (Downward weight of particles),

which can be rewritten as:

(Pressure drop across bed)(Cross-sectional area of the reactor) = (Volume of bed)(Fraction consisting of solids)(Specific weight of solids)

The above relation can be realized as a balanced equation as follows (Kunii and Levenspiel, 1991):

$$\Delta P_b A = AH(1-\varepsilon_{mf})(\bar{\rho}_s - \rho_g)g \tag{20}$$

where $\bar{\rho}_s$ is average density of particles in the system and ρ_g is density of gas mixture in the system at reaction temperature. ε_{mf} is bed voidage at minimum fluidizing conditions.

In case the number of gas molecules changes during the CVD reaction on the surface of the catalyst, one has to take into account the change in the drag force of the upward-moving gas on the left side of the Eq. (20). As depicted in Fig. 1(a), we have a model system of gas α deposited and converted to solid product β, where gas γ is produced as a by-product:

$$\alpha(g) \rightarrow \beta(s) + n_g\gamma(g) \tag{21}$$

In the expression above, n_g mole of gas γ is generated when 1 mol of gas α is deposited as the solid product β. If n_g is two, 2 mol of γ gas are generated while 1 mol of α gas disappears. However, if the conversion is 0.5, only half of the α gas reacts and thus final gas volume ($\alpha + \gamma$) should be 1.5 times higher than that of the feed gas. Therefore, gas expansion factor, δ should be defined as below:

$$\delta = 1 + (n_g - 1)X_g \tag{22}$$

According to the above relation, 1.5 of δ is obtained when X_g = 0.5 and n_g = 2, as aforementioned. As the system studied here is of very slow reaction, very low Damköhler number (Da) is expected for this system as well. At low Da number, the convective mass transfer rate overpowers the reaction rate. Therefore, the deviation of gas concentration is expected to be very low throughout the column, above minimum fluidizing condition. As the drag force increases proportional to the total number of gas molecules, the expression for the overall pressure drop with gas expansion due to the chemical reaction (ΔP_b) should be

$$\Delta P_b = \delta \Delta P_b^0 = \{1 + (n_g - 1)X_g\}\Delta P_b^0 \tag{23}$$

As the density of most gas molecules is very small compared to the solid density, with a difference of 2 ~ 3 orders of magnitude, ρ_g can be assumed to be negligible. Combining Eqs. (20) and (23) gives

$$H = \{1 + (n_g - 1)X_g\}\frac{\Delta P_b^0}{(1-\varepsilon_{mf})\bar{\rho}_s g} \tag{24}$$

The size and the density of particles change with yield, and thus, this change has to be taken into account. The average particle density, $\bar{\rho}_s$ in Eq. (24) has to be obtained by integrating over the yield change.

Let us define $\dot{\rho}_s$ as the density of the product at yield $\dot{y}$, as shown in Fig. 1(c).

An expression for $\dot{\rho}_s$ can be easily derived as follows, using the density values of both the catalyst (ρ_{cat}) and the deposited solid (ρ_{prd}).

$$\frac{\dot{\rho}_s}{\rho_{cat}} = \frac{\left(\frac{m_{cat}+m_{prd}}{V_{cat}+V_{prd}}\right)}{\left(\frac{m_{cat}}{V_{cat}}\right)} = \left(\frac{m_{cat}+m_{prd}}{m_{cat}}\right)\left(\frac{V_{cat}}{V_{cat}+V_{prd}}\right) \tag{25}$$

V_{cat} and V_{prd} indicate the volume of the catalyst and deposited solid, respectively. Note that V_{prd} is the volume of deposited product only and excludes V_{cat}, the volume of catalyst.

$$\text{As } \frac{V_{cat}+V_{prd}}{V_{cat}} = 1 + \frac{V_{prd}}{V_{cat}} = 1 + \dot{y}\frac{\rho_{cat}}{\rho_{prd}} \tag{26}$$

and with Eqs. (1) and (26), Eq. (25) can be rearranged to:

$$\dot{\rho}_s = \frac{\rho_{cat}(1+\dot{y})}{1+\frac{\rho_{cat}}{\rho_{prd}}\dot{y}} \tag{27}$$

The above expression is integrated over yield to give the average density of the particles, with the catalyst density equal to ρ_{cat} at y = 0.

$$\bar{\rho}_s = \frac{1}{y}\int_0^y \dot{\rho}_s d\dot{y} = \frac{\rho_{cat}}{y}\int_0^y \frac{1+\dot{y}}{1+\frac{\rho_{cat}}{\rho_{prd}}\dot{y}}d\dot{y} \tag{28}$$

The integration of the above expression gives

$$\bar{\rho}_s = \left(\frac{\rho_{prd}}{y} - \frac{\rho_{prd}^2}{\rho_{cat}y}\right)\ln\left(\frac{\rho_{cat}}{\rho_{prd}}y + 1\right) + \rho_{prd} \tag{29}$$

Although Fig. 1(c) only illustrates a spherical particle, the above expression for the average particle density is not limited to perfect spheres but also includes particles of low sphericity.

As $\Delta P_b^0 = \frac{\left(1+\frac{y}{2}\right)\lambda_{in}\tau g}{A}$ from Eq. (14), Eq. (24) can be rearranged to

$$H = \frac{\left(1+\frac{y}{2}\right)\lambda_{in}\tau}{(1-\varepsilon_{mf})\bar{\rho}_s A}\{1 + (n_g - 1)X_g\} \tag{30}$$

With the expression for A, the cross-sectional area of the column from Eq. (18), the above Eq. (30) becomes

$$H = \frac{u_0\rho_{f,g}\lambda_{in}\tau\left(1+\frac{y}{2}\right)\left\{X_g + (n_g-1)X_g^2\right\}}{S\bar{\rho}_s(\lambda_{out}-\lambda_{in})(1-\varepsilon_{mf})} \tag{31}$$

Combining Eq. (31) with Eqs. (2) and (29) gives

$$H = \frac{u_0\rho_{f,g}\tau X_g\left(\frac{1}{y}+\frac{1}{2}\right)\{1+(n_g-1)X_g\}}{S(1-\varepsilon_{mf})\left\{\left(\frac{\rho_{prd}}{y} - \frac{\rho_{prd}^2}{\rho_{cat}y}\right)\ln\left(\frac{\rho_{cat}}{\rho_{prd}}y+1\right) + \rho_{prd}\right\}} \tag{32}$$

or

$$H = \frac{u_0\rho_{f,g}\tau X_g\left(\frac{1}{y}+\frac{1}{2}\right)}{S(1-\varepsilon)\left\{\left(\frac{\rho_{prd}}{y} - \frac{\rho_{prd}^2}{\rho_{cat}y}\right)\ln\left(\frac{\rho_{cat}}{\rho_{prd}}y+1\right) + \rho_{prd}\right\}} \tag{33}$$

where

$$\varepsilon = \frac{\varepsilon_{mf}-1}{1+(n_g-1)X_g} + 1 \tag{34}$$

Here, ε_{mf} in Eq. (32) is bed voidage at minimum fluidization that does not consider gas expansion or shrinkage due to the catalytic reaction. ε in Eq. (33) is apparent bed voidage that considers gas volume change and thus is the one to be compared with the actual experimental or simulation results. Without gas volume changes at n_g = 1, Eq. (33) turns to an expression for minimum fluidisation, where $\varepsilon = \varepsilon_{mf}$. The relation between ε and ε_{mf} is described in Eq. (34). The bed voidage, ε in Eq. (34) goes above ε_{mf} while n_g is greater than 1. This implies that gas generation could result in gas velocity well above minimum fluidization velocity and hence result in longitudinal bed expansion, as there is no constraint of the bed top surface. On the contrary, n_g less than 1 gives ε value lower than ε_{mf}. In this case, the gas is being lost due to the CVD reaction and hence the overall bed height decreases.

From Eq. (33), one can notice that the bed height increases with the residence time, τ of the particles. This might be the case with catalysts of very poor performance that leads to very slow reaction. Although our model deals with a slow CVD reaction system, further retarded reaction rate would lead to longer residence time of the particles and hence result in more particles residing in the system. This will ultimately increase the bed height. The residence time, τ corresponding to the yield (y) used for the calculation of Eq. (19) can be obtained from a simple kinetic experiment, as mentioned in Section 2.1. The bed voidage, ε can be set based on the data from literature or obtained from a small scale lab experiment. This initial input value can be ultimately adjusted by the simulation result.

As seen from Eq. (32), one needs to increase the bed height to achieve higher conversion at a fixed production rate, which agrees well with the aforementioned argument. Note that Eq. (32) describes a minimum fluidizing bed if n_g is one or X_g is very low. In case n_g equals one, the stoichiometric ratio of input gas and exhaust gas is the same and therefore no gas expansion occurs near the catalytic site. If n_g is larger than one, the product gas volume exceeds that of reactant gas, which would lead to local bubbling near the catalytic active sites and subsequently increase overall bed height, H in Eq. (32). This observation would result in increase in apparent bed voidage, ε. Eq. (34) gives ε value of 0.6 at ε_{mf} = 0.4 when X_g = 0.5 and n_g = 2. Larger ε values result in less gap between ε and ε_{mf} values, for instance, ε of 0.69 giving ε_{mf} of 0.54. In case of excessive gas expansion, one needs to reduce input gas rate accordingly. On the contrary, if n_g is less than one, the overall gas volume would dwindle as the reactant gas undergoes catalytic reaction. In that case, one needs to adjust the gas feed rate to compensate for the loss. For instance, if the target conversion is 0.5 when n_g is zero, the system is losing half of the feed gas after the reaction and thus one may have to make up the corresponding

amount of gas with inert gas to keep the system above minimum fluidisation.

One of the advantages of the model proposed in this work is that a process engineer can easily determine the column dimension at high degree of freedom. If one understands the CVD system at hand, he or she can set their target productivity and conversion at his or her disposal. Next session discusses an example of a model system that utilizes the model proposed herein.

3. Results and discussion

3.1. Model system

Let us define a model system of carbon nanotube (CNT) synthesis using ethylene gas as the reactant. The reaction occurs at 700 °C as follows,

$C_2H_4 \rightarrow 2C(CNT) + 2H_2$

Here, the gas mole ratio n_g in Eq. (32) equals 2, and the stoichiometric ratio, S, is defined as below,

$$S = \frac{\text{mass of 1 mole } C_2H_4}{\text{mass of } C \text{ produced from 1 mole of } C_2H_4} = \frac{\text{mass of 1 mole } C_2H_4}{\text{mass of 2 mole C}} = 1.16667 \quad (35)$$

In this model system, the target yield was set to be 5 ~ 10, and the corresponding residence time was set to be 45 min (2700 s). The ε_{mf} value of 0.69 for absorption carbon (Kunii and Levenspiel, 1991) was adopted for model calculations tabulated in Tables 2, 3 and Figs. 3, 4. The material properties, such as gas density and viscosity, at 700 °C are all tabulated in Table 1. As mentioned before, the yield has to be obtained through preliminary experiments at reaction temperature, 700 °C in this case. The yield value can then give the feed rate of catalysts at the target production rate, as suggested by Eq. (2).

To prevent either sedimentation or entrainment of the particles, one needs to find the minimum fluidizing velocity and the terminal velocity, from which the superficial velocity must be determined. The value of the minimum fluidizing velocity (u_{mf}) was obtained using the expression proposed by Kunii and Levenspiel (1991).

$$\frac{1.75}{\varepsilon_{mf}^3 \varphi_s}\left(\frac{d_p u_{mf} \rho_g}{\mu}\right)^2 + \frac{150(1-\varepsilon_{mf})}{\varepsilon_{mf}^3 \varphi_s^2}\left(\frac{d_p u_{mf} \rho_g}{\mu}\right) = \frac{d_p^3 \rho_g \left(\rho_s - \rho_g\right) g}{\mu^2} \quad (36)$$

An expression for d_p in Eq. (36) can be easily derived from Eq. (26) as follows:

$$\frac{d_p}{d_{cat}} = \left(\frac{V_{cat} + V_{prd}}{V_{cat}}\right)^{1/3} = \left(1 + y\frac{\rho_{cat}}{\rho_{prd}}\right)^{1/3} \quad (37)$$

Here, ρ_{cat} corresponds to the density of the catalysts, and ρ_{prd} corresponds to the density of the CNTs. d_p indicates the average diameter of a particle bearing a catalyst in the centre and CNT growing on the surface. d_{cat} indicates the average diameter of catalysts. The viscosity of mixed gas, μ, was obtained using the expression proposed by Francis (Francis, 1958). The density of mixed gas, ρ_g, was obtained by $\rho_g = \sum x_i \rho_i$, where the density of the feed gas, C_2H_4, is 0.35 kg/m^3, and that of H_2 is 0.025 kg/m^3 at 700 °C. The mole fraction of each gas, x_i, was used at a conversion of 0.5. Although conversion can affect the values of μ and ρ_g, the u_{mf} value was found to be quite insensitive to changes in these variables. The values of μ and ρ_g at a conversion of 0 and those at a conversion of 0.5 resulted in only an approximately 0.5% difference in u_{mf} values. Calculations using Eq. (36) and the parameters in Table 1 gave a u_{mf} of 2.9 cm/s for fully grown particles at a maximum yield of 10 and conversion of 0.5.

The terminal velocity (u_t) was calculated using the expression suggested by Haider and Levenspiel (Haider and Levenspiel, 1989) as follows:

$$u_t = u_t^* \left[\frac{\rho_g^2}{\mu\left(\rho_s - \rho_g\right) g}\right]^{-1/3} \quad (38)$$

where the dimensionless terminal velocity (u_t^*) and particle diameter (d_p^*) are expressed as $u_t^* = \left[\frac{18}{\left(d_p^*\right)^2} + \frac{2.335 - 1.744\varphi_s}{\left(d_p^*\right)^{0.5}}\right]^{-1} d_p^*$ $= d_p\left[\frac{\rho_g\left(\rho_s - \rho_g\right)g}{\mu^2}\right]^{1/3}$

The terminal velocity (u_t) for raw catalysts was calculated to be 8.18 cm/s, which was also insensitive to changes in μ and ρ_g. Here, it should be stressed that the u_{mf} value was chosen for the heaviest possible CNT particles, whereas the u_t value was chosen for the lightest particles, the catalysts. Note that this work considers a continuous FBCVD system, not the transient phase where the particles are still growing to reach the maximum yield. Therefore, in steady state, some of the particles in the system have reached the maximum yield, and hence, it is irrelevant to examine the time evolution of u_{mf} and u_t due to the growth of the particles. To make sure that all the particles are properly suspended and no particles are entrained out of the system, the criterion for the superficial velocity should be a value between u_{mf} of the fully grown particles and u_t of the raw catalysts. This condition should give only a narrow process window, which is between 2.9 cm/s and 8.18 cm/s in our model system. The selected value for superficial velocity in this work was 5 cm/s, which is quite close to the u_{mf} above but also far enough to allow a reasonable margin of error. Considering that the u_t of fully grown particles was calculated to be 29.4 cm/s, the superficial velocity of 5 cm/s should be sufficient to ensure minimum fluidization behaviour.

Table 2 compares the dimensions at a conversion of 0.3 and 0.5. A conversion of 0.3 means that 30% of the input feed gas has been converted to the solid product and the remaining 70% of the unreacted gas has escaped the system through the top of the reactor. As seen from Table 2, the reactor diameter should be reduced to increase the conversion at the same production rate. Scale 1 represents a small-scale column with a production rate of 1.0E-5 kg/s, and Scale 2 represents a relatively larger-scale column with a production rate of 5.0E-5 kg/s. Fig. 3 shows the influence of the conversion on the bed height. It is clear that the bed height increases with conversion.

Table 1
Common input parameters.

Parameters	Values
u_0	0.05 m/s
X_g	0.2 ~ 0.5 g/g
ρ_{cat}	110 kg/m^3
ρ_{prd}	60 kg/m^3
S	1.16667 kg/kg
$\rho_{f.g}$	0.35 kg/m^3
ρ_s	60 kg/m^3
d_{cat}	200 μm
τ	2700 s
ε_{mf}	0.69
ϕ_s	0.8
μ	2.733E-05 Pa·s

Table 2
Mass flow rate and calculated FCVD dimensions at yield = 10.

Input	Scale-1		Scale-2	
X_g	0.3	0.5	0.3	0.5
λ_{in}(kg/s)	9.09E-07	9.09E-07	4.55E-06	4.55E-06
λ_{out}(kg/s)	1.00E-05	1.00E-05	5.00E-05	5.00E-05
D_b(cm)	5.07	3.92	11.33	8.78
H (cm)	44.99	86.52	44.99	86.52

Table 3
Comparison of FCVD dimensions at yield 5 and 10 (conversion = 0.3).

Input	Scale-1		Scale-2	
Y	5	10	5	10
λ_{in}(kg/s)	1.67E-06	9.09E-07	8.33E-06	4.55E-06
λ_{out}(kg/s)	1.00E-05	1.00E-05	5.00E-05	5.00E-05
D_b(cm)	4.85	5.07	10.85	11.33
H (cm)	49.18	44.99	49.18	44.99

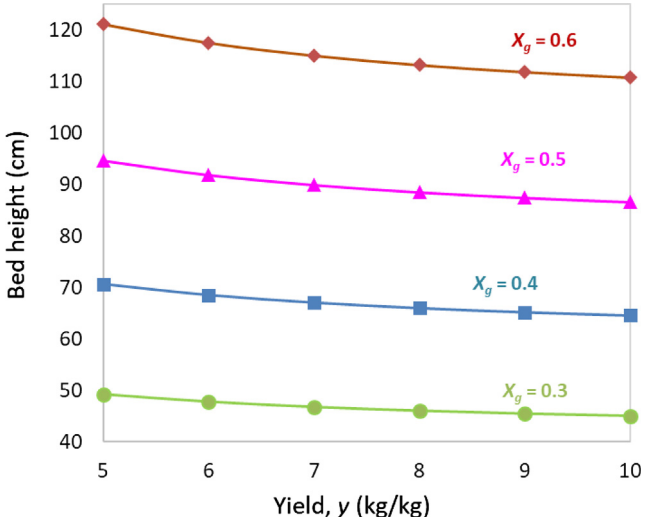

Fig. 3. Dependence of the bed height on yield at varying conversions of the feed gas.

Other important input parameters are the mass flow rates in and out of the reactor, i.e., the catalyst feed rate (λ_{in}) and production rate (λ_{out}). A higher yield at a fixed production rate should require a lower catalyst feed rate into the system. Table 3 compares the bed dimensions at yields of 5 and 10. Calculations were carried out using the parameters presented in Table 1. Table 3 shows that with a rise in yield, the column diameter slightly increases but the bed height decreases. Fig. 4(a) and (b) show the effect of conversion on the column diameter at Scale 1 and Scale 2. The results clearly show that the diameter has to be reduced to increase the conversion of feed gas. Werther (1992) also mentioned that with an increase in bed diameter, the conversion decreases due to the decrease in gas holdup.

The bed height is not affected by changes in production rate at a fixed yield, bed voidage and conversion. In other words, the bed height stays constant regardless of the production scale if the reaction conditions stay the same. This is because the superficial velocity is kept constant throughout the scale change. However, increasing only the column diameter while keeping the same height can be costly. With the same reaction conditions and the same catalysts, one way to overcome this problem is to decrease the reactor diameter by increasing the conversion, as discussed above. Let us take an example of this case. From Table 2, it can be seen that at a conversion of 0.5, scale-up from Scale 1 to Scale 2 only increases the bed diameter, not the height. The bed diameter increases from 3.92 cm to 8.78 cm, but the bed height stays the same at 86.52 cm. However, as the conversion increases from 0.3 to 0.5, the bed diameter in Scale 2 decreases from 11.33 cm to 8.78 cm, at the expense of an increase in the bed height from 44.99 cm to 86.52 cm. This strategy can save engineers from excessive expansion of the column diameter. Another way of reducing the column diameter is through increasing the superficial velocity of the feed gas. The superficial velocity, however, should be within a reasonable range below the terminal velocity to avoid vigorous bubbling behaviour. Therefore, one has to evaluate the situation at hand and manipulate process parameters carefully. If the situation requires drastic scale-up and a high production rate, one can develop a parallel arrangement of multiple small-scale FCVD reactors.

For the sake of simplicity, model verification was performed using parameters tabulated in Tables 1 and 4. For practical purposes, diameters with integer values, i.e., 5 cm and 10 cm, were chosen for model simulations, and the scales were designated as Scale 1 and Scale 2. Simulation was performed with CPFD (Bar-

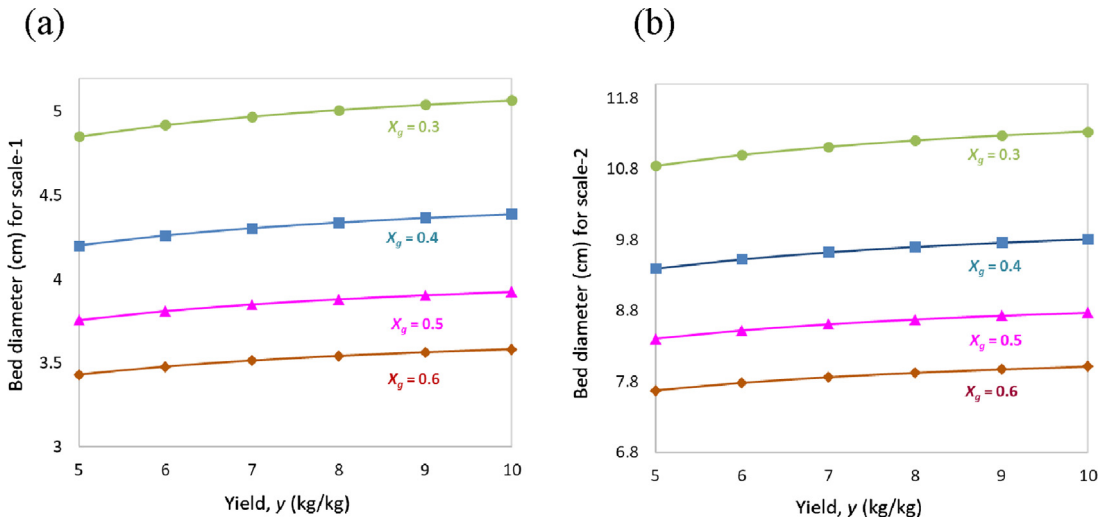

Fig. 4. Dependence of column diameter of (a) small scale and (b) large scale on the yield at varying conversions of the feed gas.

racuda 17.0.3, Windows version), and the results are presented in the following section. This work followed the same treatment as described by Shi et al. (2014) for the governing equation and the drag model for the solid phase.

3.2. Simulation results

Table 5 lists the input parameters used in the CPFD simulation. As the initial condition, the reactor was set to be filled with nitrogen gas at 700 °C and 1 atm. The total height of the FCVD reactors was set at 100 cm for both Scale 1 and Scale 2. For the chemistry input menu, the simulator was set to solve the following 3 equations simultaneously.

$$\frac{dm_{CNT}}{dt} = k_0 m_{cat} = \frac{y}{\tau} m_{cat}$$

$$\frac{dm_{C_2H_4}}{dt} = -S\frac{dm_{CNT}}{dt} = -1 \cdot 16667\frac{dm_{CNT}}{dt}$$

$$\frac{dm_{H_2}}{dt} = 2S\frac{MW_{H_2}}{MW_{C_2H_4}}\frac{dm_{CNT}}{dt} = 0 \cdot 16667\frac{dm_{CNT}}{dt} \quad (39)$$

In the above expressions, m_{cat} and m_{CNT} correspond to m_{cat} and m_{prd}, respectively, in Fig. 1(b). Additionally, MW_{H2} and MW_{C2H4} indicate the molecular mass of H_2 and C_2H_4 gas, respectively.

Note that all the units of the left-hand side and the right-hand side of the above equations are in kg/s. The simulator calculates m_{cat} with the values of density and particle diameter given in Table 1. The above expressions in Eq. (39) indicate that the rate of this reaction is almost constant, as in a zero-order reaction. Note that this model system simulates CNT growth for approximately 45 min, which is a very slow reaction. The maximum conversion to be achieved was set at 0.5, which is also quite low. In such a system, the reaction rate is almost constant, as described in the reaction kinetics and studied by Philippe et al. (2009). The productivity increases linearly with time, which is almost like a zero-order reaction. This phenomenon for CNT was also observed by Pérez-Cabero et al. (2004). They observed almost linear growth of CNT up to 100 min of reaction time, which is good enough for zero-order reaction approximation. Although the reaction rate is generally a function of the temperature and pressure of the feed gas, the pressure effect of the gas is ignored here, as the reaction rate is not limited by the mass transfer rate or mixing efficiency, but by the quality of the catalysts. The temperature effect is also ignored here as the diameters of the reactors are relatively small and thus assumed to be uniform in temperature. Overall, for a very slow reaction with a low Damköhler number, the mixing effect is often ignored, as the rate-determining factor is the reaction rate itself.

As soon as the particles, previously injected into the column at time zero, reach the target yield after the residence time of 2700 s, the simulation reaches steady state. The end time for the simulation was set at 2760, seconds with a marginal 60 s in case of data fluctuations. Fig. 5(a)~(d) demonstrate simulation results after 2700 s of the operation. The particle streams injected from above the columns observed in Fig. 5(a)~(d) represent feeding of catalysts as these systems are at continuous steady state. In case of Fig. 5(c) and (d), yellowish colour is observed near the bottom of each column, which means higher particle volume fraction due to higher yield of the particles (y = 10) near the bottom. The sparse red parts observed in Figure (b) must be from instantaneous uneven distribution of particles. Overall, Figure (a)~(d) show no signs of critical void space, which might be expressed as big chunks of blue space. Therefore, the systems presented in Fig. 5 seem to be operating at bubbling stage, above minimum fluidization and yet below slugging stage.

Table 4
Mass flow rate and calculated FCVD dimensions for model simulations.

	y = 5		y = 10	
	Scale-1	Scale-2	Scale-1	Scale-2
X_g	0.500	0.500	0.34	0.34
λ_{in}(kg/s)	2.95E-06	1.18E-05	1.01E-06	4.04E-06
λ_{out}(kg/s)	1.77E-05	7.09E-05	1.11E-05	4.44E-05
D_b(cm)	5.00	10.00	5.00	10.00

Table 5
Input parameters in the CPFD simulation.

Particle-to-particle interaction	Close pack volume fraction	0.61
	Maximum momentum redirection from collision	40%
Particle to wall interaction	Normal to wall momentum retention	0.85
	Tangent to wall momentum retention	0.85
Injection BC	Injection velocity of the catalyst	0.25 m/s
Thermal wall	Enabled	973.15 K
Chemistry	Coefficient type	Discrete
	Coefficient (k_o)	y/τ
Solver	Time step	0.01 s
	End time	2760 s

Table 6 lists the simulation results and compares them with the model predictions. The values of conversion, X_g, were obtained from the mass flow rate of ethylene gas exiting the top face of the column divided by the mass flow rate entering through the bottom face of the column. The gas flux data were set to be generated simultaneously as the simulation ran. The bed voidage (ε) values were extracted by subtracting the cell-averaged volume fraction of the bed from one. These ε values were adopted as input variables for model calculations and used to calculate ε_{mf} values through Eq. (34). All these ε and ε_{mf} values are tabulated in Table 6.

As can be seen from Fig. 5 and Table 6, the predicted values of bed height H and conversion X_g agree well with the simulation results. Compared to the model predictions, simulation gave slightly higher values of conversion and bed height, except for the case of Scale 1 at y = 5. Obviously, higher X_g values should give higher bed height, H. Therefore, increase in simulated H values could be attributed to the higher simulated conversion values, X_g. In case of Scale-1 at y = 5, however, simulation gave higher bed height than the model predicted value, even when the simulated conversion is lower than model prediction. This might be due the narrow column with high aspect ratio. The simulated aspect ratio of this system is almost 17.5, with the bed diameter and height being 5 cm and 88.4 cm, respectively. The high aspect ratio of the bed must be attributed to the pressure change due to gas generating reaction, which results in an operation well above minimum fluidization.

Werther (1992) indicated that an increase in bed diameter results in reduced gas holdup. In other words, a reduced bed diameter would result in increased gas holdup. Additionally, it is reported that a small column diameter gives significantly larger bubbles in bubbling fluidized beds (Mori and Wen, 1975). Maybe this difference in bubble size is due to the wall effect since the particles experience more contact with the wall as the column diameter decreases. This effect would be more manifested as the aspect ratio of the bed increases, due to the accumulation of gas holdup along the bed height. Therefore, one has to take extra caution when dealing with a system with relatively narrow columns.

Table 6 shows that the simulated ε values are mostly above 0.7, which is quite high. The ε_{mf} values extracted from these ε values using Eq. (34) are in the range of 0.58 ~ 0.64, also shown in Table 6. The relatively high ε_{mf} values might be due to the hairy/fluffy

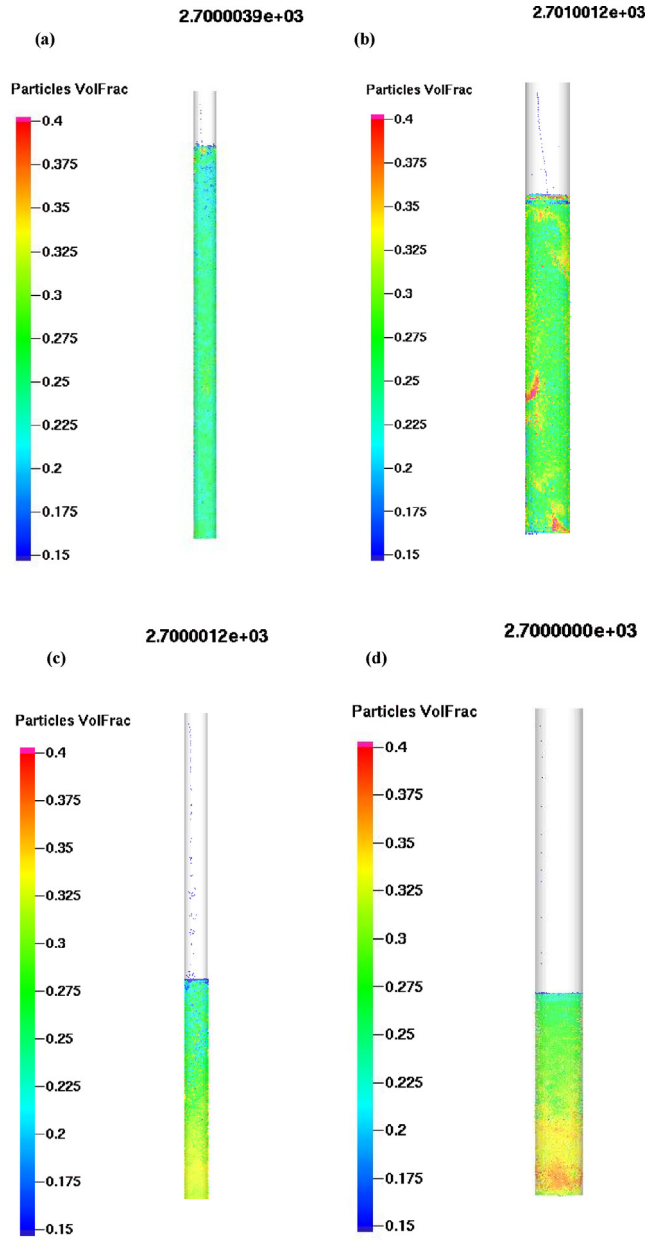

Fig. 5. CFPD simulation result of particle fluidization after residence time of 2700 s. (a) scale-1 with diameter of 5 cm and y = 5 (b) scale-2 with diameter of 10 cm and y = 5 (c) scale-1 with diameter of 5 cm and y = 10 (d) scale-2 with diameter of 10 cm and y = 10.

structure of the particles, which makes them more difficult to pack than particles of enclosed surface.

The correlations between the bed voidage and the column diameter have been reported by several researchers (Ellenberger and Krishna, 1994; Krishna et al., 1997). The authors observed that, in a dilute phase, the bed voidage is a strong function of column diameter. They also observed that the gas holdup or bed voidage decreases as the column diameter increases. As our system deals with a highly dilute system with a voidage above 0.7, the increase in voidage at low column diameters in Table 6 is justified. The problem is that it is very hard to predict the exact value of the bed voidage. There are models available that can predict the bed voidage (Hirata and Bulos, 1990; Richardson and Zaki, 1954), but such models are limited to solid–liquid fluidization systems. For a quick estimation of the bed voidage at minimum fluidization (ε_{mf}), one can perform a simple cold bed experiment or preliminary

Table 6
Simulation results.

Input & Output		y = 5		y = 10	
		Scale-1	Scale-2	Scale-1	Scale-2
Conversion X_g	Simulation results	0.45	0.53	0.36	0.36
	Model predictions	0.50	0.50	0.34	0.34
Bed voidage	Simulation results (ε)	0.76	0.72	0.72	0.69
	Model input ε	0.76	0.72	0.72	0.69
	ε_{mf}	0.64	0.58	0.63	0.58
Diameter D_b (cm)	Simulation input	5	10	5	10
	Model predictions	5	10	5	10
Bed height H (cm)	Simulation results	88.6	76.6	45.3	42.2
	Model predictions	81.4	69.8	44.0	39.5

simulation at a given column dimension with no chemistry involved.

Overall, the model prediction from this work can serve as an initial guideline for designing a steady-state continuous FCVD reactor with a slow reaction rate when only limited information including the target production rate, yield and conversion rate is available. The model presented here is aimed at direct industrial applications where all the abstruse theoretical and experimental data are not always available.

4. Conclusion

The present work suggests a simple model to determine FBCVD column dimension at a target production rate and conversion. The calculation results using the proposed model suggest that the column dimension should be adjusted depending on the conversion and the target yield of the particles. For instance, initial input value of higher conversion would result in decreased column diameter and inversely, one can seek to achieve higher conversion by decreasing column diameter at the stage of process design of the reaction column. Additionally, under the same reaction conditions at a fixed conversion and production rate, the column diameter should be increased in order to increase the yield.

The model calculations and simulation results show that the model proposed in this work agrees well with CPFD simulation results. The model is expected to serve as an initial guideline for engineers who are to design an FBCVD reactor at the basic engineering step. Additionally, it should be pointed out that the proposed model predicts the bed dimension, not the dimension of the column. Therefore, one has to give a reasonable margin to the bed height to determine the final column height, while the bed diameter should coincide with the inner diameter of the column. The model proposed in this article incorporates a term for gas volume changes due to the CVD reaction. This modelling feature enables system prediction at various reaction conditions and thus would be crucial in process optimization.

Declaration of Competing Interest

The authors declare that they have no known competing financial interests or personal relationships that could have appeared to influence the work reported in this paper.

Acknowledgement

The author thanks the Korea University of Technology and Education for providing simulation equipment and CPFD software for this research. The author would like to give special thanks to Mr. Do-Yong Lee at Kyung-Won Tech for his excellent technical assistance in CPFD simulations.

Appendix A. Supplementary material

Supplementary data to this article can be found online at https://doi.org/10.1016/j.ces.2021.116937.

References

Abbasi, A., Ege, P.E., de Lara, H.-I., 2011. CPFD simulation of a fast fluidized bed steam coal gasifier feeding section. Chem. Eng. J. 174, 341–350.
Batey, J., Tierney, E., Stasiak, J., Nguyen, T.N., 1989. Plasma-enhanced CVD of high quality insulating films. Appl. Surf. Sci. 39, 1–15.
Berenbaum, D., Duke, D.A., Hauf, H., Petri, R., Favreau, J-C., 2021. Method for depositing uniform tungsten layers by CVD, US Patent number: 6,066,366.
Breiland, W.G., Evans, G.H., 1991. Design and verification of nearly ideal flow and heat transfer in a rotating disk chemical vapour deposition reactor. J. Electrochem. Soc. 138, 1806–1816.
Breiland, W.G., Coltrin, M.E., Creighton, J.R., Hou, H.Q., Moffat, H.K., Tsao, J.Y., 1999. Organometallic vapour phase epitaxy. Mater. Sci. Eng. 24, 241–274.
Cadoret, L., Reuge, N., Pannala, S., Syamlal, M., Rossignol, C., Dexpert-Ghys, J., Coufort, C., Caussat, B., 2009. Sillicon chemical vapour deposition on macro and submicron powders in a fluidized bed. Powder Technol. 190, 185–191.
Calderbank, P.H., Toor, F.D., 1971. Fluidized beds as catalytic reactors in: Fluidization. Academic Press, London, pp. 383–429.
Caussat, B., Hemati, M., Couderc, J.P., 1995. Silicon deposition from silane or disilane in a fluidized bed – part I and II. Chem. Eng. Sci. 50, 3615–3635.
Cheng, C., Werther, J., Heinrich, S., Qi, H.-Y., Hartge, E.-U., 2012. CPFD simulation of circulating fluidized bed risers. Powder Technol. 235, 238–247.
Creighton, J.R., Ho, P., 2001. Introduction to chemical vapour deposition. In: Park, J.-H., Sudarshan, T.S. (Eds.), Chemical Vapour Deposition. ASM international, Ontario, pp. 383–429.
Ellenberger, J., Krishna, R., 1994. A unified approach to the scale-up of gas-solid fluidized bed and gas-liquid bubble column reactors. Chem. Eng. Sci. 49, 5391–5411.
Filtvedt, W.O., Javidi, M., Holt, A., Melaaen, M.C., Marstein, E., Tathgar, H., Ramachandran, P.A., 2010. Development of fluidized bed reactors for silicon production. Sol. Energy Mater. Sol. Cells 94, 1980–1995.
Filtvedt, W.O., Mongstad, T., Holt, A., Melaaen, M., Klette, H., 2013. Production of Silicon from SiH4 in a Fluidized Bed, Operation and Results. Int. J. Chem. Reactor Eng. 11, 57–68.
Francis, W.E., 1958. Viscosity equations for gas mixtures. Trans. Faraday Soc. 54, 1492–1497.
Furusawa, T., Kojima, T., Hiroha, H., 1988. Chemical vapor deposition and homogeneous nucleation in monosilane pyrolysis within interparticle spaces—application of fines formation analysis to fluidized bed CVD. Chem. Eng. Sci. 43, 2037–2042.
Guenther, C., O'Brien, T., Syamlal, M., 2001. A numerical model of silane pyrolysis in a gas-solids fluidized bed. In: the International Conference on Multiphase Flow, SRP, New Orleans, pp. 1–12.
Haider, A., Levenspiel, O., 1989. Drag coefficient and terminal velocity of spherical and nonspherical particles. Powder Technol. 58, 63–70.
Hirata, A., Bulos, F.B., 1990. Predicting bed voidage in solid-liquid fluidzation. J. Chem. Eng. Jpn. 23, 599–604.
Horio, M., Wen, C.Y., 1977. An assessment of fluidized-bed modelling. In: Fluidization Theories and Applications. American Institute of Chemical Engineers, New York, pp. 9–21.
Hua, B., Li, C., 1999. Production of characterization of nanocrystalline SnO_2 films on Al_2O_3 agglomerates by CVD in a fluidized bed. Mater. Chem. Phys. 59, 130–135.
Hua, B., Li, C., 1999. Production and characterization of nanocrystalline SnO2 films on Al2O3 agglomerates by CVD in a fluidized bed. Mater. Chem. Phys. 59, 130–135.
Jianlong, L., Guanghui, C., Pan, Z., Weiwen, W., Jihai, D., 2011. Technical challenges and progress in fluidized bed chemical vapour deposition of polysilicon. Chin. J. Chem. Eng. 19, 747–753.
King, D.M., Spencer II, J.A., Liang, X., Hakim, L.F., Weimer, A.W., 2007. Atomic layer deposition on particles using a fluidized bed reactor with in situ mass spectrometry. Surf. Coat. Technol. 201, 9163–9171.
Krishna, R., de Swart, J.W., Ellenberger, J., Martina, G., Maretto, C., 1997. Gas holdup in slurry bubble columns: Effect of column diameter and slurry concentrations. AIChE J. 43, 311–316.
Kunii, D., Levenspiel, O., 1991. Fluidization Engineering. Butterworth-Heinemann, Massachussetts.
Lee, S.-T., Lin, Z., Jiang, X., 1999. CVD diamond films: nucleation and growth. Materials Sci. Eng.. 25, 123–154.
Makris, D., Giorgi, L., Giorgi, R., Lisi, N., Salernitano, E., 2005. CNT growth on alumina supported nickel catalyst by thermal CVD. Diam. Relat. Mater. 14, 815–819.
Mills, A., Elliott, N., Parkin, I.P., O'Neill, S.A., Clark, R.J., 2002. Novel TiO_2 CVD films for semiconductor photocatalysis. J. Photochem. Photobiol., A 151, 171–179.
Mond, L., Langer, C., Quincke, F., 1890. Action of carbon monoxide on nickel. J. Chem. Soc. 57, 749–753.
Mori, S., Wen, C.Y., 1975. Estimation of bubble diameter in gaseous fluidized beds. AIChE J. 21, 109–115.
Morooka, S., Kusakabe, K., Kobata, A., 1989. Modification of submicron particles by chemical vapor deposition in fluidized bed. Fluidization VI.
Morooka, S., Okuba, T., Kusakabe, K., 1990. Recent work on fluidized bed processing of fine particles as advanced materials. Powder Technol. 63, 105–112.
Neudeck, P.G., 1995. Progress in silicon carbide semiconductor electronics technology. J. Electronic Mater. 24, 283–288.
Ni, L., Kuroda, K., Zhou, L.-P., Kizuka, T., Ohta, K., Matsuishi, K., Nakamura, J., 2006. Kinetic study of carbon nanotube synthesis over Mo/Co/MgO catalysts. Carbon 44, 2265–2272.
Parker, J., 2011. Validation of CFD model for polysilicon deposition and production of silicon fines in a silane deposition FBR. Int. J. Chem. Reactor Eng. 9, 1–18.
Partridge, B.A., Rowe, P.N., 1966. Analysis of gas flow in a bubbling fluidized bed when cloud formation occurs. Trans. Inst. Chem. Eng. 44, 349–358.
Pérez-Cabero, M., Romeo, E., Royo, C., Monzón, A., Guerrero-Ruíz, A., Rodríguez-Ramos, I., 2004. Growing mechanism of CNTs: a kinetic approach. J. Catalysis. 224, 197–205.
Philippe, R., Serp, P., Kalck, P., Kihn, Y., Bordere, S., Plee, D., Gaillard, P., Bernard, D., Caussat, B., 2009. Kinetic study of carbon nanotubes synthesis by fluidized bed chemical vapor deposition. AIChE J. 55, 450–464.
Powell, C.F., Oxley, J.H., Blocher Jr., J.M., 1966. Vapor deposition. John Wiley, NY.
Richardson, J.F., Zaki, W.N., 1954. Bed Expansion and porosity of liquid fluidised beds. Trans. Inst. Chem. Engrs. 32, 35–39.
Sanjurjo, A., Lau, K., Wood, B., 1992. Chemical vapour deposition in fluidized bed reactors. Surf. Coat. Technol. 54, 219–223.
See, C.H., Harris, A.T., 2007. A review of carbon nanotube synthesis via fluidized-bed chemical vapor deposition. Ind. Eng. Chem. Res. 46, 997–1012.
Shi, X., Lan, X., Liu, F., Zhang, Y., Gao, J., 2014. Effect of particle size distribution on hydrodynamics and solids back-mixing in CFB risers using CPFD simulation. Powder Technol. 266, 2135–2143.
Snider, D.M., 2007. Three fundamental granular flow experiments and CPFD predictions. Powder Technol. 176, 36–46.
Snider, D.M., Clark, S.M., O'Rourke, P.J., 2011. Eulerian-Lagrangian method for three-dimensional thermal reacting flow with application to coal gasifiers. Chem. Eng. Sci 66, 1285–1295.
Tejero-Ezpeleta, M.P., Buchholz, S., Mleczko, L., 2004. Optimization of reaction conditions in a fluidized-bed for silane pyrolysis. Can. J. Chem. Eng. 82, 520–529.
Wang, Q., Yang, H., Wang, P., Lu, J., Liu, Q., Zhang, H., Wei, L., Zhang, M., 2014. Application of CPFD method in the simulation of a circulating fluidized bed with a loop seal, part I - Determination of modeling parameters. Powder Technol. 253, 814–821.
Werther, J., 1992. Scale-up modeling for fluidized bed reactors. Chem. Eng. Sci. 47, 2457–2462.
Wood, B.J., Sanjurjo, A., Tong, G.T., Swider, S.E., 1991. Coating particles by chemical vapour deposition in fluidized bed reactor. Surf. Coat. Technol. 49, 228–232.
Wu, Y., Peng, L., Qin, L., Wang, M., Gao, J., Lan, X., 2018. Validation and application of CPFD models in simulating hydrodynamics and reactions in riser reactor with Geldart A particles. Powder Technol. 323, 269–283.
Zhang, Q., Zhao, M.-Q., Huang, J.-Q., Nie, J.-Q., Wei, F., 2010. Mass production of aligned carbon nanotube arrays by fluidized bed catalytic chemical vapour deposition. Carbon 48, 1196–1209.